Fall 2023

# Investigation of Inflammation and Apoptosis Mediated Toxicity in Response to Metal Oxide Nanoparticles in ML-1 and CA77 Cancer Cell Lines

Alyse N. Peters
*Missouri State University*, alyse625@live.missouristate.edu

# INVESTIGATION OF INFLAMMATION AND APOPTOSIS MEDIATED TOXICITY IN RESPONSE TO METAL OXIDE NANOPARTICLES IN ML-1 AND CA77 CANCER CELL LINES

A Master's Thesis

Presented to

The Graduate College of

Missouri State University

In Partial Fulfillment

Of the Requirements for the Degree

Master of Science, Biology

By

Alyse Peters

December 2023

**INVESTIGATION OF INFLAMMATION AND APOPTOSIS MEDIATED TOXICITY IN RESPONSE TO METAL OXIDE NANOPARTICLES IN ML-1 AND CA77 CANCER CELL LINES**

Biology

Missouri State University, December 2023

Master of Science

Alyse Peters

## ABSTRACT

Metal oxide nanoparticles (MONPs) are becoming more popular in today's environment. They contribute significantly to the technologies in agriculture and food development but there is little understanding to how MONPs, including ZnO, CuO, $TiO_2$, and $SnO_2$, impact human health and the environment. Our growth assay revealed that none of these negatively affects viability in the budding yeast, *Saccharomyces cerevisiae*. In contrast, both human thyroid cancer cells (ML-1) and rat medullary thyroid cancer cells (CA77) displayed a significant reduction in viability with the treatment of CuO and ZnO. The production of ROS in these cell lines when treated with CuO and ZnO was found to be not significantly altered. However, levels of apoptosis with ZnO and CuO were increased, which led us to conclude that the decreased cell viability is mainly caused by non-ROS-mediated cell death. Consistently, data from our RNAseq studies identified differentially regulated pathways associated with inflammation, Wnt, and cadherin signaling across both cell lines, ML-1 and CA77, after ZnO or CuO NP treatment. Results from gene studies further support non-ROS mediated apoptosis being the main factor behind decreased cell viability. Together, these findings provide unique evidence that the apoptosis in response to the treatment of CuO and ZnO in these thyroid cancer cells was not mainly due to oxidative stress but to the alteration of a range of signal cascades that promotes cell death.

**KEYWORDS**: ZnO, CuO, CA77 (rat medullary carcinoma), ML-1 (human thyroid cancer), cytotoxicity

**INVESTIGATION OF INFLAMMATION AND APOPTOSIS MEDIATED TOXICITY IN RESPONSE TO METAL OXIDE NANOPARTICLES IN ML-1 AND CA77 CANCER CELL LINES**

By

Alyse Peters

A Master's Thesis
Submitted to the Graduate College
Of Missouri State University
In Partial Fulfillment of the Requirements
For the Degree of Master of Science, Biology

December 2023

Approved:

Kyoungtae Kim, Ph.D., Thesis Committee Chair

Christopher Lupfer, Ph.D., Committee Member

Paul Durham, Ph.D., Committee Member

Julie Masterson, Ph.D., Dean of the Graduate College

## ACKNOWLEDGEMENTS

Thank you to Dr. Kyoungtae Kim, who tremendously helped me during my time at Missouri State University. His advice and patience carried me through all the stages of writing my thesis. His dedication and enthusiasm inspired me to be the best researcher I can be.

To my committee members, Dr. Christopher Lupfer and Dr. Paul Durham. I am grateful for your brilliant comments and suggestions through the process of my thesis and my educations at MSU.

I would also like to thank Rishi Patel for providing relevant input and feedback on this project. I am indebted to the U.S. Army Engineer Research and Development Center-Environmental Laboratory (ERDC-EL) for supporting my work.

I dedicate this thesis to Darrin Peters. Thank you for inspiring my love for science and to keep persevering.

## TABLE OF CONTENTS

## LIST OF TABLES

## LIST OF FIGURES

# INTRODUCTION

Metals such as gold, silver, titanium, copper, zinc, and aluminum have all been used to synthesize nanomaterials, as well as their oxides, i.e., silver oxide, copper oxide, magnesium oxide, calcium oxide, and zinc oxide. These common nanomaterials exhibit magnetic, fluorescence quenching, and dielectric properties [1,2]. In particular, MONPs are no more than 100 nm in size and are one of the most studied nanomaterials against multidrug-resistant bacteria [3, 4]. Importantly, the small size of MONPs increases the surface/volume ratio, which improves their stability and the ability to interact with different cellular components [5]. Furthermore, MONPs are very popular because of their lower price and simple synthesis process [6].

Many researchers have uncovered the antibacterial properties of MONPs, which can make an impact on bacterial growth and reproduction [7]. Infectious bacterial cells accumulate on hospital bed sheets, patient gowns, and uniforms, and can be one of the main causes of hospital-acquired infections (HAIs). To combat HAIs, CuO, ZnO, and $TiO_2$ MONPs of different sizes were all tested on *S. aureus*, *B. subtilis*, *P. aeruginosa*, and *E. coli* [7]. Among the tested MONPs, ZnO and CuO MONPs caused the greatest decrease in cell viability in bacterial strains. In particular, CuO MONPs of 10–14 nm caused decreased viability in *S. aureus* and *B. subtilis*, while ZnO NPs of 12- 15.5 nm caused decreased viability in *P. aeruginosa* and *E. coli* [7]. Overall, all the MONPs tested clearly had the ability to counteract the proliferation of bacterial strains. Frenk et al. assessed CuO and $Fe_2O_3$ in a study to understand the potential impact of these MONPs on soil-living bacteria and found that CuO has a more severe negative impact on hydrolytic activity and soil oxidative potential [8]. Both CuO and $Fe_2O_3$ used in the study were about the same size (smaller than 50 nm), and therefore, this investigation has limited

information on the impact of MONP size on cell toxicity. Zhang et al. evaluate $TiO_2$ with several different sizes on human epidermal keratinocytes and found that only $TiO_2$ of 27.5 nm induced modest cytotoxicity compared to larger particles [9]. A similar study focused on the shape of MONPs rather than size; they compared rod-shaped and sphere-shaped $Fe_2O_3$ and CuO [10]. From this study, both rod-shaped $Fe_2O_3$ and CuO exhibited more toxic effects on cell viability and ROS production than spherical MONPs [10]. They proposed that the greater surface area of rod-shaped MONPs compared to spherical MONPs is the main cause of the increased toxicity [10].

In vitro cell culture is a useful tool to gain insight into underlying toxicity mechanisms. Many researchers are concerned with MONPs' (ZnO, CuO, $TiO_2$, and $SnO_2$, specifically) impact on human health and the environment [11]. A recent study evaluated $TiO_2$ on different aquatic cell lines (RTG-2, PLHC-1, RTH-149, and RTL-W1) and tested their cytotoxicity [12]. The mitochondria activity, plasma membrane integrity, and lysosome function in each cell line stated above after $TiO_2$ treatment (100 µg/mL and lower) were detected to be normal [12], indicating low cytotoxicity of $TiO_2$ MONPs. Similarly, $SnO_2$ was reported to have negligible cytotoxic effects [13]. Ahamed et al. investigated $SnO_2$, concentrations ranging from 10–200 µg/mL, on breast cancer MCF-7 cells [13]. Interestingly, $SnO_2$ alone conveyed no toxic effects but when paired with ZnO nanocomposite ($SnO_2$-ZnO/rGO NPs) the resulting toxicity was greatly increased [13]. In contrast to the previously reported non-toxic effects of $TiO_2$ and $SnO_2$, ZnO NPs are one of the most toxic MONPs. In a 2019 study, HaCaT keratinocytes were treated with ZnO MONPs and showed increased toxicity due to the dissolution of $Zn^{2+}$ ions, emphasizing that the cytotoxicity is caused by the ability of ions to internalize by endocytosis [14]. Similarly,

Mahmood et al. stated that CuO MONPs elicit significant cytotoxicity in MCF-7 cells by activating the apoptotic signal cascade [15].

Given that CuO and ZnO led to more toxicity over $TiO_2$ and $SnO_2$ against mammalian cells as stated above, most researchers gave attention to the study of the toxic mechanisms in response to ZnO and CuO MONPs in both in vitro and in vivo experiments. However, these MONPs' impact on animal and human thyroid cancer cells has not been documented at all. In addition, the literature on MONP's effects on fungal cells is scarce. Therefore, we evaluated the toxic impact of MONPs such as ZnO, CuO, $TiO_2$, and $SnO_2$, against two thyroid cancer cell lines, ML-1 (human thyroid cancer) and CA77 (rat medullary thyroid carcinoma), and the budding yeast *Saccharomyces cerevisiae* to obtain broader understanding to the cytotoxicity of MONPs and their potential environmental implications.

MONPs are becoming an everyday part of life, but environmental consequences need to be considered. There are 4 main sources in which MONPs can enter the environment, manufacturing, nano-enabled products, product use, and the biggest culprit waste management. It is evident from many studies that MONPs in excess are harmful to plants, aquatic organisms, and mammalian cell lines. Increasing MONPs in the environment may cause serious agricultural issues in the future as well as poorly understood effects in mammalian cell lines. I decided to test 4 MONPs including $TiO_2$, $SnO_2$, CuO and ZnO NPs to ML-1 and CA77 cells to uncover toxicity mechanisms. Based on past literature reporting metal oxide-based cell toxicity, I hypothesize that these MONP will affect the viability of ML-1 and CA77 cells by an elevation of reactive oxygen species (ROS) and an induction of ROS-mediated apoptosis in the presence of these MONPs. My last hypothesis is that MONPs will cause alteration of several signaling pathways relating to apoptosis and inflammation.

# METHODS

## ZnO and CuO NP Scanning Transmission Electron Microscopy (STEM)

Four metal oxide nanoparticles (ZnO, CuO, $SnO_2$, and $TiO_2$) were purchased from US Research Nanomaterials, Inc (TX, USA). These MONPs (1 mg/mL) were received as they are dispersed in water. Only ZnO and CuO showed viability decrease, therefore we decided to proceed with just these two nanoparticles for the following experiments. A JEOL 7900F Scanning Electron Microscope (SEM) with a Scanning Transmission Electron Microscopy (STEM) detector was used to image the CuO and ZnO nanomaterials. The 2 samples CuO (40 nm) and ZnO (35-45 nm) were diluted to a concentration of 0.1 mg/mL and were subsequently drop cast onto holy carbon film TEM grids and allowed to air dry in a desiccator box. All physicochemical experiments in this thesis were conducted at the Jordan Valley Innovation Center at Missouri State University with the help of Rishi Patel, a senior scientist in the Center for Applied Science and Engineering, unless otherwise stated.

## X-ray Diffraction of ZnO and CuO NPs

X-ray diffraction (XRD) was conducted using a Bruker D2 phaser XRD system to characterize the crystallinity of CuO and ZnO nanomaterials. Both nanomaterials were prepared similarly, wherein a few milligrams of the dry nanoparticles were dispersed in methanol. The paste was then coated on a zero-background silicon plate and dried on a hotplate at 75ºC for 10 min.

## Yeast Culture and Viability Assay

Budding yeast *Saccharomyces cerevisiae* strain S288C was grown in 2X synthetic-defined glucose (2X SD+Glu) media and placed in a shaking incubator at 30℃ to grow overnight. The optical density (OD) was taken of the liquid cell culture at 594 nm and recorded to be used in the cell stock calculation. The cell stock of the inoculated cell culture was diluted to get 0.2 OD. Each of the nanomaterials used, ZnO, CuO, $TiO_2$, and $SnO_2$, was independently suspended in water at a concentration of 1,000 µg/mL. A nanoparticle stock solution was made for each of the four treatment groups by combining the suspended nanomaterial with molecular-grade water to a final concentration of 200 µg/mL. Two trials were performed for each of the four nanoparticle treatment groups.

A round-bottom 96-well plate was utilized in this experiment to get the most accurate OD reading. Typically, round-bottom plates are used for yeast suspension. A 1:2 serial dilution was performed of the nanoparticle stock solution to provide treatment conditions ranging from 0 µg/mL to 100 µg/mL. Yeast cells were then added to only the first 3 rows of the seeded wells leaving the bottom 3 rows to be a comparative control only containing nanomaterial and 2X SD+Glu media. Each of the treatment concentrations and their corresponding control was seeded 3 times on the 96-well plate. The seeded plate was then placed in a BioTek ELx808 Absorbance Microplate Reader where the OD was read at 594 nm every 30 minutes over a period of 24 hours. This series of experiments were conducted in triplicate and repeated 3 times. Data shown are one representative of reproducible data collected.

**Statistical Analysis**

The OD obtained from the treated wells was subtracted from the corresponding control wells without cells to get a corrected OD. Each plate tested the varying concentrations in

triplicate which were averaged after the corrected OD was found to create growth curves representing each test concentration. GraphPad Prism9 was used to perform a one-way ANOVA statistical analysis to determine if the treated samples were statistically significantly different from the non-treated samples. Endpoint graphs were made using the OD at the 24-hour mark and asterisks were used to identify values significantly different ($p$-value < 0.05). Dunnett's multiple comparisons were used to visualize the variance in control and treatment groups. The graph bars represent an average of three replicates and error bars represent standard deviation. Statistically significant data are represented as *p<.05, **p<.01, ***p<.001, ****p<.0001. Triplicate experiments were repeated multiple times to confirm reproducibility.

**Cell Cultures**

ML-1 cells were purchased from DSMZ, German collection of Microorganisms and Cell Cultures. CA77 cells were obtained from Jordan Valley Innovation center (JVIC) from Dr. Paul Durham (Missouri State University) and maintained in DMEM with 10% FBS, 5% penicillin and 5% amphotericin. Both cell lines were cultured in 95% $O_2$ and 5% $CO_2$ incubator. Mouse fibroblast cells were obtained from Dr. Chris Lupfer (Missouri State University) and maintained in same conditions.

**XTT Cell Viability**

An XTT assay was performed on ML-1 (human thyroid cancer) and CA77 (rat thyroid cancer) cells to explore the viability of ZnO, $TiO_2$, CuO, and $SnO_2$ nanoparticles. A flat bottom 96-well plate was used for cell culture in order for the cells to adhere to the bottom of the plate. Using a flat bottom 96-well plate, 10,000 ML-1 cells were seeded per well and incubated in a

37℃ incubator for 24 hours. On day two, DMEM media (Dulbecco's Modification with 4.5g/L glucose, L-glutamine and sodium pyruvate purchased from Corning) was removed from each well and then replaced with 100 µL fresh DMEM. ML-1 (and CA77) cells now have adhesion to the bottom of the wells. DMEM media was removed from designated treatment wells and 120 µL of stock nanoparticle mix (MONP + DMEM) was added to each well for a final concentration of 100 µg/mL of MONPs. For one nanoparticle, four wells would receive stock chemical mix making the total volume 480 µL (120µL per each well). A serial dilution was conducted by removing 20 µL from wells containing the 120 µL of treatment stock and replaced into the next well. This is repeated until final concentrations are 100 µg, 20 µg, 4 µg with a dilution factor of 5 for each nanoparticle. Each well has a final volume of 100 µL and is treated in triplicate. A positive control, dimethyl sulfide, was also done in triplicate with concentrations of 5%, 10% and 20%. Treated cells were incubated for another 24 hours. After incubation, a 1:200 XTT solution was prepared containing XTT buffer (both buffer and reagent purchased from Biotium; buffer cat: 30007) and XTT activation reagent (PMS, Biotium). Each well was treated with 25 µL of the prepared XTT stock for 7 hours at 37℃. Absorbance measurements are most accurate during this time frame. The BioTek ELx880 Absorbance Microplate Reader measures the formazan dye formed in each well. This analysis was repeated for mouse fibroblast cells and CA77 rat thyroid cancer cells.

**Calculation of $IC_{50}$ Value**

The $IC_{50}$ value represents when 50% of cells were inhibited in cell viability. AAT Bioquest website was used (https://www.aatbio.com/tools/ic50-calculator). Data from ML-1 cells were inserted into the equation to determine $IC_{50}$ values; it was determined that ZnO's $IC_{50}$

was 22.8 µg/mL and CuO's $IC_{50}$ value was 45.5 µg/mL. The $IC_{50}$ value was then calculated for CA77 cells from XTT cell viability data. These values were as follows: 67.98 µg/mL for ZnO and 72.88 µg/mL for CuO.

**Reactive Oxygen Species (ROS)**

Two separate 24-well plates were seeded with 50,000 ML-1 and CA77 cells per well and placed into an incubator for 24 h at 37°C, after the cells were cultured and counted. The following day, DMEM was removed from each well and replaced with pre-warmed DMEM. ZnO and CuO were used for this experiment because of their XTT cell viability assay results that showed a significant decrease in cell proliferation. The designated $IC_{50}$ value for ZnO (22.8 µg/mL) was treated into the labeled wells. CuO at 45.5 µg/mL was treated into the labeled column of three wells. These treatments were conducted in triplicate as well as the positive control (DMSO) treated at 20%, and an untreated control. An untreated control group and two blanks (no Dehydroethidium, DHE) were only treated with DMEM. The third day consists of washing treated cells once with 500 µL 1x phosphate-buffered saline (PBS; OmniPur). To detach the cells, 250 µL trypsin+EDTA was added to each well and then placed in the incubator for 15 minutes. After the incubation period, trypsin+EDTA is neutralized with 500 µL pre-warmed DMEM. The cell suspension in each well was transferred to labeled 2 mL centrifuge tubes to be centrifuged for 10 min at 400 x g. During this time, the ROS indicator, DHE (dehydroethedium, purchased from ThermoFisher), was prepared by mixing 26 µL DHE into 26 mL 1x PBS in a 50 mL Falcon tube. Given DHE being light sensitive, the 50 mL Falcon tube containing indicator mix was covered with aluminum foil. The supernatant from the centrifuge tubes was removed and 1mL of indicator mix was added to each tube except the two blanks. The two blanks

received 1mL PBS. After pipetting up and down, each resuspended mix was transferred to new, foil-covered 2 mL centrifuge tubes. Cells were then incubated for 1 hour before being analyzed by Attune NxT Flow Cytometer. The dyed samples were measured at 518/606nm.

**CellROX Green Reactive Oxygen Species (ROS)**

Detaching and counting cells must be finished before seeding plates. Three separate 18-well plates were seeded with 10,000 ML-1 cells per well. Each 18-well plate was for a different time period, 4 hours, 24 hours, and 48 hours. After 24 hours of incubation, all plates are treated with the $IC_{50}$ values of both ZnO and CuO. Four treatment groups were conducted in triplicate: NTC, ZnO, CuO, and 10% $H_2O_2$, which was used as a positive control. Four hours after treatment, cells were washed with 100 µL of 1 x PBS, and then CellROX green solution was applied. Five µM of CellROX green dye was added to each well. Following the CellROX green dye treatment, cells were washed 3 times with a live imaging solution to make sure phenol red from DMEM does not interfere. Immediately, cells were visualized with a confocal microscope. We chose 10 cells randomly with detectable fluorescence to evaluate the fluorescence intensity with ImageJ. Greater fluorescence positively correlates to greater ROS. Images were taken at different time points.

**Apoptosis**

For the experiment, an Annexin-V binding buffer as well as two dyes, Propidium Iodide and Annexin V-APC (BD Biosciences), were used for apoptotic measurement. The 10x Annexin V binding buffer was made by combining 0.1 M of HEPES, 1.5 M sodium chloride (NaCl), 25 mM of calcium chloride ($CaCl_2$), and molecular-grade sterile water. An 1x Annexin V binding

buffer solution was made by diluting 18 mL of PBS and 2 mL of the 10x Annexin V binding buffer. Initially, 50,000 ML-1 or CA77 cells were seeded per well in a 24-well plate and then incubated for 24 hours. After the incubation period, DMEM was replaced and then NPs were added into each well. Concentrations of 22.8 µg/mL ZnO and 45.5 µg/mL CuO were tested in triplicate along with DMSO and a NTC group. In order to calibrate the flow cytometer, 3 blanks, also with 50,000 ML-1 cells per well, were prepared. On day three, each well was washed with 300 µL 1x PBS and then 250 µL trypsin (25%, 2.21mM) without EDTA was pipetted into each well. The plate was placed in an incubator for 20 minutes while the cells detached. To neutralize the non-EDTA trypsin, 300 µL of fresh DMEM was added into each well and then pipetted up and down. The treatment groups, NTC, and DMSO groups were resuspended in 100 µL Annexin V binding buffer solution, 5 µL Annexin V-APC, and 5 µL propidium iodide (50 µg/mL), then incubated in the dark for 30 minutes. After the incubation, an additional 400 µL Annexin V binding buffer solution was added to each sample. Final analysis of each sample was based on the excitation properties of the dyes. Annexin V emits at 660 nm with a red laser and propidium iodide emits at 617 nm with a blue laser. Apoptosis experiments were conducted in triplicate and repeated three independent times.

**Total RNA Extraction**

Extracting RNA requires four different phases: homogenization, separation, isolation, and washing according to Invitrogen TRIzol protocol (Ambion, Carlsbad CA 92008). RNA extraction was conducted on CA77 cells as well as ML-1 cells. On the first day, 750,000 CA77 cells were seeded into each well of a 6-well plate. Two 6-well plates were used for a total of 9 samples: three NTC, three 68.9 µg/mL ZnO treated, and three 73 µg/mL CuO treated. For ML-1

cells, ZnO at 22.8 µg/mL and CuO at 45.5 µg/mL CuO were tested. After 24 hours of incubation followed by 24 hours of incubation with $IC_{50}$ values of ZnO and CuO, total RNA was extracted. For this, 1 mL of TRIzol was added to homogenize the cells. Each sample was incubated for 5 minutes to complete dissociation of the nucleoprotein complex. Next, each sample was incubated with 200 µL chloroform for 2-3 minutes. After centrifugation, three phases formed: an upper colorless, an intermediate, and a lower red phase. The colorless phase contains RNA. The colorless phase was acquired and then 100% isopropanol was added in equal parts. After another centrifugation, the supernatant was removed containing RNA and 1 mL of 75% EtOH was added to each Eppendorf tube. Finally, ethanol was removed, and tubes were left in the biosafety cabinet until completely dry. Thirty µL nuclease-free water was added to each tube to make total RNA concentration of 2 µg total and was shipped to Kanas University Medical Center for production of cDNA library and RNA seq studies.

**RNA Seq Analysis**

After receiving files from Kansas University Medical Center, files were uploaded to *Basepair*. The spike-in ERCC was used when uploading files to reduce variability and identify errors. There was a linear correlation between the known concentration, expected concentration, and read counts for each of the different probes. Linear correlation indicates good sample quality. The first step in the RNA-seq pipeline was trimming to remove the poor quality of reads as well as adapter sequences. Each read was aligned to STAR, which is the reference genome to accurately identify the source of the gene. After all reads were aligned, Feature Counts was used for expression quantification to look at each gene and how many mapped reads are aligned to that specific gene. Next, the differential gene expression analysis step involved statistical

analysis to find changes in gene expression between each sample group. DESeq2 tool was used for differential expression analysis. After differential expression analysis, a volcano plot displays genes with log10 p-value. A heat map was used to indicate up- and down- regulated genes. Genes were sorted with fold change of 2.01 and -2.01 with *p*-adjusted value less than 0.05. The 5 most up or downregulated genes were chosen and investigated with IDTdna and Gorilla. CLC genomics was used for CA77 cells to identify the differentially-regulated genes when treated with ZnO and CuO. Datasets were downloaded, unzipped, then transported into CLC genomics. Fastq files were uploaded and then concatenated in *Galaxy*. After quality checks, RNA-seq analysis was conducted on each sample and CA77 gene expression was analyzed using CLC genomics.

# RESULTS

## Scanning Transmission Electron Microscopy (STEM) with ZnO and CuO NPs

As stated in the method section, $TiO_2$ and $SnO_2$ had no significant impact on cell viability, so we decided to focus on investigating the physicochemical properties of CuO and ZnO for the current study. Scanning Transmission Electron Microscopy (STEM) images for each nanomaterial which approximate the CuO and ZnO nanomaterial size in agreement with that of the data sheet values; 40 nm and 35-45 nm respectively (**Figure 1**).

## X-ray Diffraction of ZnO and CuO NPs

Using Bruker's Evaluation software, the peaks were identified as the material based on the miller index and peak fitting. Once the correct file that fits the data most accurately was selected the Crystallographic Information File was then fitted to the experimental data to confirm that each nanomaterial (CuO and ZnO) matched the standard file, respectively. **Figure 2** provides the Xray diffraction plot (XRD) plots for each of the nanomaterials tested.

## Yeast Viability Was Not Compromised by the Treatment of ZnO, CuO, $TiO_2$, and $SnO_2$

Absorbance-based growth assays were performed to better understand the potential toxicity of ZnO, CuO, SnO2, and TiO2 on the biological organism Saccharomyces cerevisiae. After analyzing the optical density of MONP-treated cells at 594 nm over a period of 24 h, we found that all MONPs did not reduce the growth of Saccharomyces cerevisiae at concentrations up to 100 μg/mL (**Figure 3A–H**). Rather, as shown in **Figures 3B,F**, ZnO and SnO2 caused slightly increased growth when compared with non-treated groups (0 μg/mL). These results are

expected because budding yeast has a cell wall which is hypothesized to be a protective layer that keeps MONPs from accessing cell cytoplasm.

**XTT Cell Viability Assay**

To investigate which metal nanoparticles, ZnO, CuO, TiO2, or SnO2, are potentially harmful to ML-1 thyroid cancer cells, an XTT cell viability assay was conducted. ML-1 cells were incubated with concentrations of 4 µg/mL, 20 µg/mL, and 100 µg/mL for each of the four MONPs. After 7 h of incubation with an XTT activation reagent, ML-1 viability correlates to measured absorbance levels. Five groups (100 µg/mL of ZnO, 100 µg/mL of CuO, and all three DMSO groups) showed $p < 0.001$ as compared with non-treated control (NTC). In particular, at the concentration of 100 µg/mL, both ZnO and CuO nanoparticles had significantly decreased cell viability (**Figure 4**). Based on this XTT assay, ZnO and CuO were chosen as the most toxic nanoparticles out of the four and were used for the following experiments. .

Two MONPs, ZnO and CuO, showed markedly decreased cell viability when treated to ML-1 cells (**Figure 4**). To determine IC50 values, differing amounts (20 µg/mL, 40 µg/mL, 60 µg/mL, 80 µg/mL, and 100 µg/mL) of both ZnO and CuO were treated to ML-1 cells (**Figure 5A**). After 7 h of incubation with an XTT activation reagent, cells with 40 µg/mL of ZnO displayed a significantly decreased cell viability ($p < 0.01$), while 60 µg/mL of CuO had a comparable level of viability reduction to 40 µg/mL of ZnO-treated cells (**Figure 5A**, $p < 0.05$). Using the AAT Bioquest website, we determined IC50 values of ZnO and CuO for ML-1 cells: 22.8 µg/mL for ZnO and 45.5 µg/mL for CuO.

CA77 rat medullary thyroid carcinoma cells displayed similar levels of viability loss when compared to that of ML-1 human thyroid cancer. A comparison of these two cell lines can

give an insight as to which cell line is more sensitive to MONP treatment. An additional XTT cell viability was conducted on CA77 cells with a similar treatment: 20 µg/mL, 40 µg/mL, 60 µg/mL, 80 µg/mL, and 100 µg/mL for both ZnO and CuO (**Figure 5B**). A concentration of 20 µg/mL for both CuO and ZnO was the lowest concentration in which the viability of CA77 cells was inhibited **(Figure 5B**, $p < 0.05$). The next higher concentrations of these MONPs also caused decreased cell viability, with statistically significant p values (**Figure 5B**, $p < 0.01$). IC50 values were calculated in a manner identical to that with the ML-1 cells: 68.2 µg/mL of ZnO and 72.8 µg/mL of CuO for CA77 cells.

Incubation of MONPs with mouse fibroblast cells can help determine if they could be used as an anticancer treatment. An important aspect of cancer therapy we should consider before its application to cancer is if they are able to target only cancer cells. If MONPs also lead to a reduction in fibroblast cell viability, then they would be a poor option for anti-cancer treatment. It was found that fibroblast cells showed decreased cell viability with ZnO treatment (**Figure 5C**, $p < 0.05$). However, CuO NPs showed similar trends compared to NTC. ML-1 cells were determined to be the most sensitive to ZnO and CuO treatment compared to CA77 cells.

**Reactive Oxygen Species (ROS)**

Reactive Oxygen Species (ROS) are free radicals that largely contribute to disturbing the cell in stressful environments. Superoxide level was tested in ML-1 and CA77 cells using dihydroethidium (DHE). Cells were treated for 24 h with IC50 values of ZnO and CuO calculated for ML-1 cells; 22.4 µg/mL of ZnO or 45.5 µg/mL of CuO. Samples were incubated with DHE and measured with flow cytometry. Observing the fluorescence intensity of DHE of each cell sample, we determined the percentage of cells with oxidative stress. Three samples for each

treatment group were averaged to visualize the differences between them. A solution of 20% DMSO was used as a positive control (**Figure 6A–D**). In the ML-1 treatment for 24 h with ZnO or CuO, ROS production was not statistically significantly different compared to the non-treated control (**Figure 6A**). Median fluorescent intensity showed an increase in superoxide production for the positive control ($p < 0.05$) (**Figure 6B**), but no significant alteration in superoxide production for both treatments (22.4 μg/mL of ZnO and 45.5 μg/mL of CuO) (**Figure 6B**). ML-1 cells were then treated for 4 h with these MONPs because 24 h of incubation with these MONPs resulted in a cell viability decrease (**Figures 4 and 5**), which possibly indicates that superoxide levels could be elevated at an earlier time point. However, even a 4 h (**Figure 6C**) or a 30 min treatment (**Figure 6D**) with ZnO or CuO resulted in no significant alteration of superoxide levels. CA77 cells were treated with 68.9 μg/mL of ZnO and 72.3 μg/mL of CuO for 24 h (**Figure 6E**), revealing no significant alteration in levels of superoxide upon the treatments.

**Reactive Oxygen Species (ROS) Levels Measured with CellROX Green**

Reactive Oxygen Species **(**ROS) can come from many areas in the cell. CellROX green is another fluorogenic probe used for measuring oxidative stress in live cells, reporting levels of ROS including superoxide and hydroxyl radicals. ML-1 cells treated with 22.8 μg/mL of ZnO and 45.5 μg/mL of CuO had essentially no significant impact on levels of ROS both at 24 h (**Figure 7A**) and 48 h of incubation (**Figure 7B**) with these MONPs. After 24 h of MONP treatment, CA77 cells display no significant elevation of ROS (**Figure 7C**), whereas both ZnO ($p < 0.01$) and CuO ($p < 0.001$) treatments for 48 h (**Figure 7D**) in CA77 cells resulted in the elevation of oxidation stress.

**Apoptosis**

Although ML-1 cells (**Figures 6**) and CA77 cells showed no significant increase in ROS after 24 h treatment of ZnO and CuO, a potential mechanism behind the decreased cell viability (**Figures 4 and 5**) that we saw in earlier XTT experiments would be apoptosis. To test this possibility, we tested both thyroid cancer cell lines with the above-stated IC50 values for ZnO and CuO (**Figure 8A,B**). ML-1 cells showed an increase both in early and late apoptosis with the increased average percentage of cells in either phase of apoptosis (**Figure 8A**, $p < 0.01$), although ZnO-treated cells were not statistically significantly different from the non-treated control group due to a high standard error (**Figure 8A**). Interestingly, in CA77 cells, the majority of apoptosis cells with MONPs are in an early stage of apoptosis (**Figure 8B**, $p < 0.0001$), while ML-1 cells are under a late apoptotic phase in the same treatment. Together, both cells display an elevated induction of apoptosis within 24 h of treatment with these MONPs.

**Altered Genome with ZnO and CuO NP Treatment of ML-1 Cells**

RNAseq data were aligned with the human genome, which resulted in a total of 19,000 differentially regulated genes when treated with ZnO or CuO in ML-1 cells. However, only 271 upregulated genes and 327 downregulated genes from the ZnO-treated cells were not excluded by a two-fold cut-off threshold and a p-value less than 0.05. Our GO term analysis revealed that the most frequently upregulated pathways include p53, Wnt signaling, CCKR, and Gonadotropin hormone receptor pathway (**Table 1**, the column labeled as "Up by ZnO"). A few of the most highly upregulated genes, with at least a 20-fold increase in their transcripts, include metal-response genes (MT2A and ZNF100) and genes involved in the p53 pathway (MYC and CCNA2). Interestingly, cell-cell adhesion, inflammation, and Wnt signaling pathways were found to be the most frequently downregulated (**Table 1**, the column labeled "Down by ZnO").

Consistently, our analysis displayed the most significantly downregulated genes (more than a 20-fold decrease in their transcripts) with ZnO treatment, including CDH16, a gene implicated in the cell adhesion pathway. In addition, CYP17A1 and CYP2E1, implicated in cytochrome p450 monooxygenase metabolism, were significantly downregulated in our analysis.

After CuO treatment, the most frequently upregulated pathways include Wnt, gonadotropin-releasing hormone, and CCKR pathway (**Table 1**, the column labeled "Up by CuO"). Among many, the following six transcripts were most significantly upregulated (more than 20-fold): POLE, PCNA, DUSP5, SPRY1, PTPRK, and MTUS1. In particular, POLE and PCNA are implicated in DNA replication, while MTUS1 is known to be involved in cell proliferation. The most frequently downregulated pathways include Wnt, inflammation, and cadherin signaling pathway (**Table 1**, the column labeled "Down by CuO"). Genes that were most significantly downregulated (more than 20-fold) included PCDH15, GNAT1, TENM2, DYRK2, HMOX1, and KIAA1001. It was found that PCDH15 and TENM2 are known to be associated with cell adhesion regulation, consistent with the most frequently downregulated pathways. Together, it was found that genes implicated in DNA replication were highly upregulated, while genes whose functions are implicated in cell adhesion are significantly downregulated.

**Altered Genome with ZnO and CuO NP Treatment on CA77 Cells**

CA77 cells treated with ZnO NPs had 256 genes upregulated and 136 genes downregulated. The most frequently upregulated pathways include the thyrotrophin-releasing hormone receptor signaling pathway, inflammation, and Wnt signaling (**Table 1**, the column labeled "Up by ZnO" in CA77 cell). The three most highly upregulated genes were found to be

Lmx1b (regulating protein binding to DNA), Ccr5 (inflammation), and Rtkn2 (apoptotic signaling). Downregulated pathways after ZnO NP treatment include integrin signaling pathways, inflammation, and cytoskeletal regulation (**Table 1**, the column labeled "Down by ZnO" in CA77 cells). The three most severely downregulated genes were found to be Bad (apoptosis), Nlrp10 (immune response), and Bag6 (autophagy). Together, this result suggests that both inflammation and apoptotic mechanisms are not balanced with the ZnO treatment in CA77 cells.

CA77 cells treated with CuO NPs expressed 118 upregulated genes and 163 downregulated genes. Most of the upregulated genes were not distinctive biological pathways. There were only three main upregulated pathways: TGF-beta signaling, interleukin signaling, and inflammation mediated by chemokine and cytokine signaling pathways (**Table 1**, the column labeled "Up by CuO" in CA77 cells). The three most highly upregulated genes were found to be Aox4 (Xenobiotic function), Dpp4 (collagen binding), and Pdcd1Ig2 (cytokine regulation). In contrast, inflammation mediated by chemokine and cytokine signaling pathways, angiogenesis, and VEGF signaling were the most frequently downregulated pathways affected by CuO treatment (**Table 1**, the column labeled "Down by CuO" in CA77 cells). The three most severely downregulated genes in our analysis were Stx11 (interferon signaling), Frat1 (Wnt signaling), and Pglyrp4 (humoral immune response).

## DISCUSSION

The present study provides novel insights into the molecular mechanisms underlying MONPs-mediated toxicity. Given the large quantity of MONPs discharged after their use, all organisms from prokaryotes to the most complex eukaryotes have been exposed to these materials. The toxicity of MONPs was addressed through many different methods in this study including cell viability, ROS, apoptosis, and RNAseq. To start, yeast, ML-1, CA77, and fibroblast cells were all used to quantify cell viability. Initially, yeast cells were treated for 24 h with $TiO_2$, $SnO_2$, ZnO, or CuO. There was no significant viability decrease in yeast cells (**Figure 3**), which is substantially different from mammalian viability trends (**Figures 4 and 5**). The structure of yeast compared to mammalian cells is very different. One of the main distinctions is the cell wall component, which could be a major factor as to why the MONPs are not hurting growth.

Most current literature focuses on cervical, breast, and lung cancers but investigating human thyroid cancer (ML-1) can be a unique discovery in the field. Not only are ML-1 cells rarely studied but comparing toxic effects in human thyroid cells with those in rat thyroid cells can give more insight into which MONPs exert more toxicity. Finally, we used fibroblast cells to check if these NPs can be used as alternative cancer therapy as previously discussed in the literature [16] One of the major conundrums in our study is ROS results. Based on recent literature [17, 18], increased ROS is the main cause of decreased cell viability after MONP treatment. Unlike the usual trend, we saw insignificant ROS production consistently in both thyroid cancer cell types for the first 24 h after treatments. Because of this result, we decided to use two different methods to quantify ROS (DHE and CellROX green) to confirm our results.

DHE experiments showed insignificant changes in ROS with both cell lines (**Figure 6**) after 24 h, 4 h, or even 30 min. DCF was used on ML-1 cells to reevaluate levels of ROS, but the same trend was evident after 24 h (Data not shown). Interestingly, CA77 cells displayed an increased level of ROS at 48 h (**Figure 7**), though ML-1 cells showed no increased ROS, leading us to believe there is a different mechanism in place behind decreased cell viability after treatment. Kalhson et al. demonstrated alternative mechanisms behind cell death upon MONP treatment. For example, excess Zn2+ ions can cause nonapoptotic cell death by inhibiting ATP synthase [19]. Interestingly, copper toxicity is also linked to altered mitochondrial function [19] through protein aggregation at the mitochondria, thus most likely impairing the energy production process occurring in the organelle. Another unique contribution of the present study is that the RNAseq analysis offers a plethora of novel explanations for non-ROS-mediated pathways that lead to cell death. Accordingly, the present study proposes that ZnO affects several pathways of the cellular stress response, which leads to cell death. Similarly, we concluded that differentially expressed genes implicated in the DNA replication process and inflammation in CuO-treated cells are the main mechanisms of cell death.

**Both ZnO and CuO Lead to Reduction in Cell Viability**

Lines of research, in which a range of cancer cells have been used for their research, have suggested MONPs as anticancer therapy agents [16]. Although cancer cells are surrounded by non-cancerous cells in vivo, many published papers fail to include normal tissue cells as a control experiment in their research. For example, Bai and colleagues reported that MONPs induce a significant level of cytotoxicity in cancerous cells without mentioning the effects of their impact on regular tissue cells [20]. To elucidate the impact of MONPs in normal tissue

cells, our study included mouse fibroblast cells along with two cancer cell lines, ML-1 and CA77. One interesting finding from our analysis is that ZnO NPs caused significant viability defects in the fibroblast cells (**Figure 5C**), while CuO-treated cells demonstrated no significant viability defect. Consistently with our ZnO-treated viability defects, Teng Ng and Yong used human fibroblast cells (MRC5) treated with ZnO NPs and observed a significant dose-dependent viability decrease [21]. Together, it is considered that ZnO NPs make them a poor candidate for cancer therapy. Out of the four MONPs (SnO2, TiO2, ZnO, and CuO), ZnO and CuO only had obvious toxic effects when treated to ML-1 cells, CA77 cells, and mouse fibroblast cells by showing significantly decreased cell viability.

ML-1 cells represent human thyroid cancer, which is an excellent model for developing how MONPs function in vitro. ML-1 cells are very rarely researched compared to other cancer cell lines including CA77 cells. In our XTT viability experiment, ML-1 cells showed viability defects with ZnO concentration as low as 40 μg/mL (**Figure 5A**). CuO-treated ML-1 cells showed viability defects starting at 60 μg/mL of CuO (**Figure 5A**). From these results, IC50 values were calculated to be 22.4 μg/mL for the ZnO-treated culture and 45.5 μg/mL for the CuO-treated culture. Although we found that IC50 values calculated in several reports were significantly different depending on the cell lines used, ranging from 10 to 100 μg/mL of ZnO. However, a few reports, including Namvar et al. that used mouse breast cancer (4Ti) treated with ZnO NPs, revealed their corresponding IC50 values very close to the IC50 values we reported here [22]. Another popular cancer cell line, MOLT4, was evaluated with CuO NPs and produced an IC50 value of 38.41 μg/mL [23]. Given the comparably low IC50 values in ML-1 cells as compared with other sensitive cell lines (4Ti and MOLT4) to ZnO and CuO, we came to the conclusion that ML-1 cells can be categorized as a highly sensitive cell line to these MONPs.

Evaluating the viability of CA77 cells can give further insight into animal models affected by ZnO and CuO treatment. CA77 cells treated with CuO and ZnO have a similar decreased cell viability pattern to ML-1 cells (**Figure 5B**). However, CA77 cells appear to be more resistant to these MONP treatments based on their higher IC50 values compared to those of ML-1 cells. After ZnO and CuO treatment, 50% of cells were inhibited in viability at 68.9 μg/mL and 72.9 μg/mL, respectively (**Figure 5B**). To compare, B9 rat cancer cell lines were used by Kukia and Abbasi and treated with CuO MONPs. B9 cells displayed significantly lower IC50 values (12.01 μg/mL) after CuO NP treatment, making them very susceptible to MONPs [24]. Varying IC50 values are expected after the treatment depending on how different cancer cells react. Based on our results, CA77 cells showed decreased cell viability even with a higher concentration of ZnO and CuO than ML-1, indicating that CA77 cells are more resistant than ML-1 to these MONPs.

**Levels of Reactive Oxygen Species (ROS) Were Not Altered Between Treatment with $IC_{50}$ Values**

Elevated levels of Reactive Oxygen Species (ROS) can often lead to decreased cell viability as previously shown [25, 26]. ROS are natural byproducts of cellular oxidative metabolism and play an important role in cell survival, cell death, differentiation, cell signaling, and inflammation-related factor production [27]. Our ROS experiments were inconsistent with current literature trends. Both ML-1 and CA77 cell lines (**Figure 6**) treated with ZnO and CuO for 24 h showed essentially no changes in the levels of superoxide. The modestly altered levels of ROS between treatments were not statistically significantly different from one another (**Figure 6**). Similarly, after 4 h or 30 min of treatment, the superoxide production level in both

ML-1 and CA77 cell lines was similar to the level of superoxide in non-treated control cells (**Figure 6**). We hypothesized that superoxide in our experiments could have been elevated as soon as we treated cells with these MONPs. However, ROS elevation was not observed even 30 min after the treatment of CuO and ZnO (**Figure 6**). Therefore, our finding is not consistent with a 2020 paper that evaluated total levels of ROS in Gingival squamous cancer cells (GSCC) [27], including superoxide, and that discovered elevated superoxide upon short-term exposure to ZnO MONPs (30–60 min). When it comes to the treatment of CuO, Bondarenko et al. detected superoxide using DHE and concluded that among MONPs tested, CuO was one of the greatest superoxide producers [28]. Together, although many reports have argued that increased ROS is the mechanism behind decreased cell viability, the observation of cell viability defects in our experiments with ZnO and CuO does not seem to be due to elevated ROS.

**Apoptosis Was Induced Both in ML-1 and CA77 Cells with MONPs**

Apoptosis is the process behind programmed cell death. No discernable alteration in ROS levels (**Figure 6**) with viability defects (**Figure 5**) in response to MONPs (24 h treatment) suggests that non-ROS-mediated apoptosis could be the main factor behind the observation. In light of the finding of increased late apoptosis in ML-1 cells and increased early apoptosis in CA77 cells after 24 h of incubation with the IC50 values of ZnO and CuO MONPs (**Figure 8**) points to ML-1 being less resistant to the treated MONPs. Other researchers investigated non-ROS-mediated apoptosis with ZnO NPs. They found that the dissolution of Zn2+ ions from ZnO MONPs can lead to an imbalance in homeostasis, then damage to lysosomes and mitochondria, and finally cell death [29]. ZnO MONPs are popularly used as drug delivery systems that can be designed to bind to specific receptors on the membrane. The binding of these nanomaterials to

death receptors may lead to cell death by inducing a signal complex, which cleaves caspase 3 and activates caspase 8 [30]. Our current study emphasizes non-ROS mediated apoptosis after ZnO and CuO treatment to both cell lines (ML-1 and CA77).

**Upregulated Transcripts Implicated in p53 and Wnt Pathways After ZnO Treatment of ML-1 cells**

After analyzing differentially expressed genes (DEGs) in ZnO-treated ML-1 cells, p53 and Wnt signaling pathways were not only frequently (**Table 1**) but also highly upregulated (**Figure 9**). Two of the most upregulated genes involved in the p53 pathway include MYC and CCNA2. It is well-known that the p53 pathway is activated in response to stress signals like DNA damage [31]. Given that a group of researchers recently found that ZnO (50 μg/mL) induces DNA damage in A549 (human lung carcinoma) cells [32], we conjecture that the ZnO treatment in our experiments might have resulted in DNA damage, which then upregulated the transcripts in the p53 pathway. It appears that a similar DNA damage response occurs as treated with ZnO in different organisms. For example, in a recent study, CCNA2 was also upregulated in D. melanogaster after ZnO treatment [26]. The upregulation of the p53 pathway in ZnO-treated cells is highly consistent with the increased late apoptosis observed in our apoptosis results (**Figure 8**).

In addition, SMAD5 and CDH1 are implicated in the Wnt signaling function that regulates cell growth, differentiation, and cell death. SMAD5 was found to be a tumor suppressor candidate [33] and CDH1 is a tumor suppressor, too [34]. Both genes were upregulated based on our RNAseq analysis after ZnO treatment in ML-1 cells (**Table 1**). Similarly, it was found by Salesa et al. that CDH1 was also upregulated in HaCaT cells after

ZnO treatment [35]. The upregulation of these tumor suppressor genes in our experiments may likely be correlated to low cell growth in ZnO-treated cells due to the inhibition of cell proliferation, as backed up by our XTT viability analysis (**Figures 4 and 5A**).

**Severely Downregulated Genes Include Inflammation and Cadherin Signaling After ZnO Treatment in ML-1 cells**

The most severely downregulated gene discovered in the ZnO-treated ML-1 cells are connected with cadherin signaling (CDH16) and xenobiotic metabolism (**Figure 9**). Consistent with our study, a 2020 study evaluated ZnO NPs in human tenon fibroblast cells (HTFs) and found downregulation of the E-cadherin pathway [36]. Given cadherin plays a role in the growth and cell-cell adhesion, the downregulation of CDH16 suggests that ML-1 cells treated with ZnO NPs could lose cell-cell adhesion and growth properties.

**Genes Implicated in DNA Repair and Growth Inhibition Were Significantly Upregulated After CuO Treatment to ML-1 Cells**

We found that gene transcripts implicated in growth inhibition were significantly upregulated: SPRY1, DUSP5, and MTUS1 (**Figure 10**). In particular, MTUS1, a known tumor suppressor involved in Wnt signaling [37], and therefore, the upregulation of it is correlated with an inhibition of cell growth, which we observed in **Figures 4 and 5**.

DNA repair pathway genes were found to be significantly upregulated in our experiments: PCNA and POLE, (**Figure 10**). Since lines of investigation including Martinez et al. point to DNA damage by the presence of CuO in cells [23], the upregulated DNA repair pathway reflects DNA damage in response to CuO treatment in the present study. One

interesting, downregulated gene shown in our model (**Figure 10**) is HMOX1, which is known to act against oxidative stress [38], suggesting no elevation of ROS in our CuO treatment experiments. Therefore, this RNAseq result of the low transcript of HMOX1 is consistent with our non-ROS-mediated cell growth defects.

**Wnt Signaling and Cadherin Pathways Were Downregulated After CuO Treatment to ML-1 Cells**

Downregulated pathways after CuO treatment are very similar to downregulated pathways with ZnO treatment to ML-1 cells. For example, Wnt signaling (WNT7B) is downregulated (**Figure 10**). As mentioned previously, the downregulation of Wnt pathways can lead to inhibited proliferation [39]. Therefore, the growth defect in ML-1 cells in response to CuO is in part due to the downregulation of cell proliferation by Wnt signaling. In addition, both PCDH15 and TENM2, associated with cadherin signaling, were also downregulated in our experiment (**Figure 10**). Therefore, it is considered that the downregulation of adhesion signaling might further exacerbate the growth potential of ML-1 cells in the presence of CuO.

**Inflammation is the Most Upregulated Pathway After CuO Treatment to CA77 Cells**

After CuO MONP treatment to CA77 cells, inflammation was the most frequently upregulated pathway (**Table 1**). In addition, we found that Dpp4, a modulator of inflammation [40], was significantly (>20-fold) upregulated in CA77 cells with the present study (**Figure 11**). Pcd1l2g is another inflammatory gene upregulated in CA77 cells after treatment (**Figure 11**). It is clear that CuO MONPs cause increased inflammation as reported many times in the recent literature [41-43]. Given that CuO MONPs can bind to cell death ligands to induce non-ROS-

mediated apoptosis [44], our RNAseq studies further confirm non-ROS-mediated apoptosis through increased inflammation pathways.

**Severely Downregulated Angiogenesis and Cadherin Pathways After CuO treatment to CA77 Cells**

After CuO treatment, the few, most severely downregulated genes shown in **Figure 11** are Clec9a and Il10rb (cytokine pathway), and Frat1 (Wnt signaling). In particular, Frat1 mainly functions as a positive regulator of Wnt signaling and regulates tumor progression [45]. Given that Wnt signaling is widely known for promoting cell proliferation, our data on the severe downregulation of the Wnt signaling factor suggest growth defects in the presence of CuO.

**Genes Involved in Inflammation Pathways Were Significantly Upregulated After ZnO Treatment to CA77 Cells**

Genes involved in inflammation were found to be upregulated (more than a 20-fold increase) after ZnO MONP treatment in CA77 cells: Ccr5 and Zfp36l1 (**Figure 12**). It is known that ZnO MONPs induce inflammation as reported many times, especially in mammalian cells [46-48]. Therefore, in CA77 cells, it appears that Ccr5 and Zfp36l1 upregulation in response to ZnO treatment takes place to promote inflammation.

Ackr3, associated with inflammation, was downregulated severely after ZnO treatment to CA77 cells (**Figure 12**). Anti-inflammatory mechanisms were discussed in a paper by Agarwal and Shannmaug [49]. They explained that ZnO NPs used for drug delivery functions can elicit anti-inflammatory properties like stability characteristics.

Integrin is involved in cell-cell and cell-extracellular matrix adhesion [50], and we found that integrin pathways are severely downregulated after ZnO NP treatment to CA77 cells (**Figure 12**). The cd2 gene is implicated in the integrin pathway and was downregulated significantly (**Figure 12**). From our current studies, 24 h of treatment causes CA77 cells to detach from the bottom of the flask. Additionally, Fernández and colleagues evaluated ZnO MONPs and found a similar result [51].

## Conclusion

After analyzing our RNAseq data, many differentially regulated pathways over-lapped after ZnO and CuO treatment in both cell lines (ML-1 and CA77). Briefly, both CuO and ZnO MONPs altered inflammation, cadherin, Wnt signaling, and p53 pathways in ML-1 cells. Similarly, CA77 cells exhibited altered Wnt, inflammation, and angiogenesis pathways after both treatments with ZnO or CuO. Therefore, animals and humans have similar pathways altered after ZnO or CuO treatment. Though these altered pathways are similar, the genes differentially regulated varied in each cell line. The biggest common denominators between both cell lines were found to be inflammation and Wnt signaling. These findings further confirm non-ROS-mediated apoptosis being the mechanism be-hind decreased cell viability in our experiments. Together, ZnO and CuO NPs cause dysregulation in inflammation, which could be the main factor behind increased apoptosis and decreased cell viability.

## Limitations

It is important to note that most ROS experiments were conducted at 24 hours. To get a more accurate conclusion regarding ROS, it would be beneficial to conduct additional

experiments after 30 minutes to an hour of MONP treatment. Cell density is another factor to consider when conducting any experiment in a 96, 24, 12 or 6 well plate. A denser plate of cells could have less of an effect than a less dense seeded well plate.

## REFERENCES


1.Nikolova, M.P. and M.S. Chavali, Metal Oxide Nanoparticles as Biomedical Materials. Biomimetics (Basel), 2020. 5(2).

2.Pan, S., et al., Therapeutic Applications of Metal and Metal-Oxide Nanoparticles: Dermato-Cosmetic Perspectives. Front Bioeng Biotechnol, 2021. 9: p. 724499.

3.Chai, H., et al., The effect of metal oxide nanoparticles on functional bacteria and metabolic profiles in agricultural soil. Bull Environ Contam Toxicol, 2015. 94(4): p. 490-5.

4.Nino-Martinez, N., et al., Molecular Mechanisms of Bacterial Resistance to Metal and Metal Oxide Nanoparticles. Int J Mol Sci, 2019. 20(11).

5.Wang, C., et al., Metal oxide gas sensors: sensitivity and influencing factors. Sensors (Basel), 2010. 10(3): p. 2088-106.

6.Stankic, S., et al., Pure and multi metal oxide nanoparticles: synthesis, antibacterial and cytotoxic properties. J Nanobiotechnology, 2016. 14(1): p. 73.

7.Azam, A., et al., Antimicrobial activity of metal oxide nanoparticles against Gram-positive and Gram-negative bacteria: a comparative study. Int J Nanomedicine, 2012. 7: p. 6003-9.

8.Frenk, S., et al., Effect of metal oxide nanoparticles on microbial community structure and function in two different soil types. PLoS One, 2013. 8(12): p. e84441.

9.Zhang, L.W. and N.A. Monteiro-Riviere, Toxicity assessment of six titanium dioxide nanoparticles in human epidermal keratinocytes. Cutan Ocul Toxicol, 2019. 38(1): p. 66-80.

10.Lee, J.H., et al., Rod-shaped iron oxide nanoparticles are more toxic than sphere-shaped nanoparticles to murine macrophage cells. Environ Toxicol Chem, 2014. 33(12): p. 2759-66.

11.Zhu, Y., et al., Recent advances in the biotoxicity of metal oxide nanoparticles: Impacts on plants, animals and microorganisms. Chemosphere, 2019. 237: p. 124403.

12.Bermejo-Nogales, A., et al., Negligible cytotoxicity induced by different titanium dioxide nanoparticles in fish cell lines. Ecotoxicol Environ Saf, 2017. 138: p. 309-319.

13.Ahamed, M., et al., SnO(2)-Doped ZnO/Reduced Graphene Oxide Nanocomposites: Synthesis, Characterization, and Improved Anticancer Activity via Oxidative Stress Pathway. Int J Nanomedicine, 2021. 16: p. 89-104.

14.Singh, S., Zinc oxide nanoparticles impacts: cytotoxicity, genotoxicity, developmental toxicity, and neurotoxicity. Toxicol Mech Methods, 2019. 29(4): p. 300-311.

15.Mahmood, R.I., et al., Biosynthesis of copper oxide nanoparticles mediated Annona muricata as cytotoxic and apoptosis inducer factor in breast cancer cell lines. Sci Rep, 2022. 12(1): p. 16165.

16.Vinardell, M.P. and M. Mitjans, Antitumor Activities of Metal Oxide Nanoparticles. Nanomaterials (Basel), 2015. 5(2): p. 1004-1021.

17.Li, Y., et al., Mechanism of photogenerated reactive oxygen species and correlation with the antibacterial properties of engineered metal-oxide nanoparticles. ACS Nano, 2012. 6(6): p. 5164-73.

18.Kessler, A., et al., Reactive Oxygen Species Formed by Metal and Metal Oxide Nanoparticles in Physiological Media-A Review of Reactions of Importance to Nanotoxicity and Proposal for Categorization. Nanomaterials (Basel), 2022. 12(11).

19.Kahlson, M.A. and S.J. Dixon, Copper-induced cell death. Science, 2022. 375(6586): p. 1231-1232.

20.Bai, D.P., et al., Zinc oxide nanoparticles induce apoptosis and autophagy in human ovarian cancer cells. Int J Nanomedicine, 2017. 12: p. 6521-6535.

21.Ng, C.T., et al., Zinc oxide nanoparticles exhibit cytotoxicity and genotoxicity through oxidative stress responses in human lung fibroblasts and Drosophila melanogaster. Int J Nanomedicine, 2017. 12: p. 1621-1637.

22.Namvar, F., et al., Cytotoxic effects of biosynthesized zinc oxide nanoparticles on murine cell lines. Evid Based Complement Alternat Med, 2015. 2015: p. 593014.

23.Angele-Martinez, C., et al., Reactive oxygen species generation by copper(II) oxide nanoparticles determined by DNA damage assays and EPR spectroscopy. Nanotoxicology, 2017. 11(2): p. 278-288.

24.Kukia, N.R., A. Abbasi, and S.M.A. Froushani, Copper Oxide Nanoparticles Stimulate Cytotoxicity and Apoptosis in Glial Cancer Cell Line. Dhaka Univ. J. Pharm. Sci., 2018. 17(1): p. 105-111.

25.Jeong, S.H., et al., ZnO nanoparticles induce TNF-alpha expression via ROS-ERK-Egr-1 pathway in human keratinocytes. J Dermatol Sci, 2013. 72(3): p. 263-73.

26.Cardozo, T.R., et al., Genotoxicity of zinc oxide nanoparticles: an in vivo and in silico study. Toxicol Res (Camb), 2019. 8(2): p. 277-286.

27.L, S.W., et al., ZnO Nanoparticles Induced Caspase-Dependent Apoptosis in Gingival Squamous Cell Carcinoma through Mitochondrial Dysfunction and p70S6K Signaling Pathway. Int J Mol Sci, 2020. 21(5).

28.Bondarenko, O., et al., Toxicity of Ag, CuO and ZnO nanoparticles to selected environmentally relevant test organisms and mammalian cells in vitro: a critical review. Arch Toxicol, 2013. 87(7): p. 1181-200.

29.Kao, Y.Y., et al., Zinc oxide nanoparticles interfere with zinc ion homeostasis to cause cytotoxicity. Toxicol Sci, 2012. 125(2): p. 462-72.

30.Kadhem, H.A., et al., Zinc Oxide Nanoparticles Induces Apoptosis in Human Breast Cancer Cells via Caspase-8 and P53 Pathway. Nano Biomedicine and Engineering, 2019. 11(1): p. 35-43.

31.Williams, A.B. and B. Schumacher, p53 in the DNA-Damage-Repair Process. Cold Spring Harb Perspect Med, 2016. 6(5).

32.Freire, K., et al., Cytotoxicity and DNA damage evaluation of TiO(2) and ZnO nanoparticles. Uptake in lung cells in culture. Toxicol Res (Camb), 2021. 10(2): p. 192-202.

33.Fuchs, O., et al., Inhibition of Smad5 in human hematopoietic progenitors blocks erythroid differentiation induced by BMP4. Blood Cells Mol Dis, 2002. 28(2): p. 221-33.

34.Song, M.S., et al., Nuclear PTEN regulates the APC-CDH1 tumor-suppressive complex in a phosphatase-independent manner. Cell, 2011. 144(2): p. 187-99.

35.Salesa, B., I.S.R. Sabater, and A. Serrano-Aroca, Zinc Chloride: Time-Dependent Cytotoxicity, Proliferation and Promotion of Glycoprotein Synthesis and Antioxidant Gene Expression in Human Keratinocytes. Biology (Basel), 2021. 10(11).

36.Wang, L., et al., Zinc oxide nanoparticles induce human tenon fibroblast apoptosis through reactive oxygen species and caspase signaling pathway. Arch Biochem Biophys, 2020. 683: p. 108324.

37.Cheng, L.Y., et al., MTUS1 is a promising diagnostic and prognostic biomarker for colorectal cancer. World J Surg Oncol, 2022. 20(1): p. 257.

38.Sebastian, V.P., et al., Heme Oxygenase-1 as a Modulator of Intestinal Inflammation Development and Progression. Front Immunol, 2018. 9: p. 1956.

39.Kahlert, U.D., et al., Pharmacologic Wnt Inhibition Reduces Proliferation, Survival, and Clonogenicity of Glioblastoma Cells. J Neuropathol Exp Neurol, 2015. 74(9): p. 889-900.

40.Baggio, L.L., et al., Plasma levels of DPP4 activity and sDPP4 are dissociated from inflammation in mice and humans. Nat Commun, 2020. 11(1): p. 3766.

41.Pietrofesa, R.A., et al., Copper Oxide Nanoparticle-Induced Acute Inflammatory Response and Injury in Murine Lung Is Ameliorated by Synthetic Secoisolariciresinol Diglucoside (LGM2605). Int J Mol Sci, 2021. 22(17).

42.Tulinska, J., et al., Copper Oxide Nanoparticles Stimulate the Immune Response and Decrease Antioxidant Defense in Mice After Six-Week Inhalation. Front Immunol, 2022. 13: p. 874253.

43.Wang, K., et al., Respiratory Exposure to Copper Oxide Particles Causes Multiple Organ Injuries via Oxidative Stress in a Rat Model. Int J Nanomedicine, 2022. 17: p. 4481-4496.

44.Jiang, Y., et al., Copper-induced tumor cell death mechanisms and antitumor theragnostic applications of copper complexes. Nanomedicine (Lond), 2022. 17(5): p. 303-324.

45.van Amerongen, R. and A. Berns, Re-evaluating the role of Frat in Wnt-signal transduction. Cell Cycle, 2005. 4(8): p. 1065-72.

46.Roy, R., et al., Mechanism of uptake of ZnO nanoparticles and inflammatory responses in macrophages require PI3K mediated MAPKs signaling. Toxicol In Vitro, 2014. 28(3): p. 457-67.

47.Jung, A., et al., Effect of Pulmonary Inflammation by Surface Functionalization of Zinc Oxide Nanoparticles. Toxics, 2021. 9(12).

48.Huang, K.L., et al., Zinc oxide nanoparticles induce eosinophilic airway inflammation in mice. J Hazard Mater, 2015. 297: p. 304-12.

49.Agarwal, H. and V. Shanmugam, A review on anti-inflammatory activity of green synthesized zinc oxide nanoparticle: Mechanism-based approach. Bioorg Chem, 2020. 94: p. 103423.

50.Bachmann, M., et al., Cell Adhesion by Integrins. Physiol Rev, 2019. 99(4): p. 1655-1699.

51.Fernandez-Cruz, M.L., et al., Comparative cytotoxicity induced by bulk and nanoparticulated ZnO in the fish and human hepatoma cell lines PLHC-1 and Hep G2. Nanotoxicology, 2013. 7(5): p. 935-52.

Table 1. Altered Pathways with Differentially Expressed Genes (DEG) by ZnO or CuO in ML-1 and CA77 Cells. Each well has a number of DEG implicated in the biological pathway listed in the column of "Pathways with DEG". Altered pathways with high frequency are indicated in red; in particular, a large number of Wnt and inflammation signaling pathway genes are up- or down-regulated by ZnO and CuO.

| Pathways with DEG | ML-1 Cells | | | | CA77 Cells | | | |
|---|---|---|---|---|---|---|---|---|
| | Up by ZnO | Down by ZnO | Up by CuO | Down by CuO | Up by ZnO | Down by ZnO | Up by CuO | Down by CuO |
| Gonadotrophin-releasing hormone receptor | 13 | 5 | 6 | 2 | 1 | | | 3 |
| CCKR signaling | 13 | 3 | 5 | | 1 | 1 | | |
| Wnt signaling | 12 | 7 | 6 | 7 | 3 | 2 | | |
| P53 | 12 | | | | 1 | 2 | | |
| Nicotine degradation/nicotine acetylcholine receptor | 11 | | | 6 | 2 | 1 | | 2 |
| Huntington disease | 11 | 2 | 2 | | 2 | 2 | | |
| Integrin signaling | 10 | 5 | 4 | 4 | 2 | 4 | | |
| Inflammation | 10 | 7 | | 6 | 3 | 4 | 2 | 7 |
| Apoptosis | 9 | 2 | 3 | 2 | 1 | 1 | | |
| PDGF signaling | 8 | | 2 | | 1 | 1 | 1 | |
| Heterotrimeric G-protein signaling | 8 | 6 | | 10 | 6 | 2 | | 3 |
| Angiogenesis | 8 | | 4 | 3 | | 2 | | |
| Presenilin (Alzheimer) | 8 | | 2 | 3 | 1 | 2 | | |
| Parkinson disease | 7 | | | | | 1 | | |
| TGF-beta signaling | 6 | | 2 | 2 | | | 1 | |
| Cadherin signaling | 6 | 7 | | 6 | | 1 | | |
| Cytoskeletal regulation by Rho GTPase | 5 | | | | 3 | 2 | | |
| Glutamate receptor groups I, I, III | 5 | | | 5 | 2 | | | 1 |
| Ionotropic glutamate receptor | 4 | | | | | | | |
| FGF signaling | 4 | 2 | | 2 | 1 | 1 | | 1 |
| EGF receptor signaling | 4 | 3 | | | 1 | 1 | | 1 |
| DNA replication | 4 | | | | | | | |
| Plasminogen activating cascade | 4 | | | | | | | |
| Blood coagulation | 4 | 3 | | | 1 | | | 1 |
| B cell activation | 4 | 2 | | | | 1 | | |
| Adrenaline and noradrenaline biosynthesis | 3 | | | | | | | |
| Endothelin | 3 | | | | | | | |

Table 1 continued. Altered Pathways with Differentially Expressed Genes (DEG) by ZnO or CuO in ML-1 and CA77 Cells. Each well has a number of DEG implicated in the biological pathway listed in the column of "Pathways with DEG". Altered pathways with high frequency are indicated in red; in particular, a large number of Wnt and inflammation signaling pathway genes are up- or down-regulated by ZnO and CuO.

| Pathways with DEG | ML-1 Cells | | | | CA77 Cells | | | |
|---|---|---|---|---|---|---|---|---|
| | Up by ZnO | Down by ZnO | Up by CuO | Down by CuO | Up by ZnO | Down by ZnO | Up by CuO | Down by CuO |
| Axon guidance | 3 | | | | | | | |
| PI3K kinase | 3 | | 2 | 2 | | | | |
| Oxidative stress response | 3 | | 2 | | | | | |
| Notch Signaling | 3 | | 3 | | 2 | | | |
| Amyloid secretase | | 2 | | | | | | |
| Interleukin signaling | | | 2 | 3 | | | 1 | |
| Dopamine receptor | | | | 3 | 1 | 1 | | |
| Opioid | | | | 4 | 1 | | | 1 |
| VEGF signaling | | | | | 2 | 2 | | 3 |
| Thyrotrophin-releasing hormone receptor | | | | | 4 | | | |
| JAK-STAT | | | | | 1 | 1 | | |

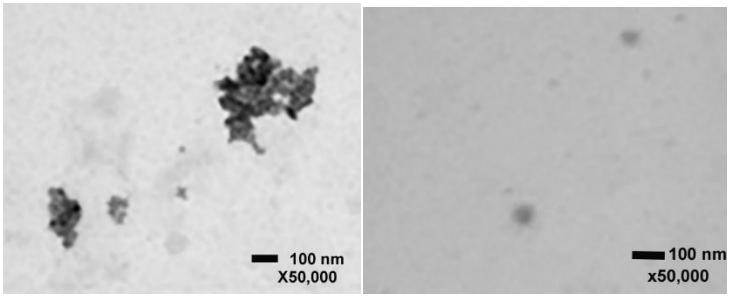


Figure 1. Scanning Transmission Electron Microscopy (STEM) Images of CuO (left) and ZnO (right) at High (50,000×) Magnifications. Bars on the images represent 100 nm.

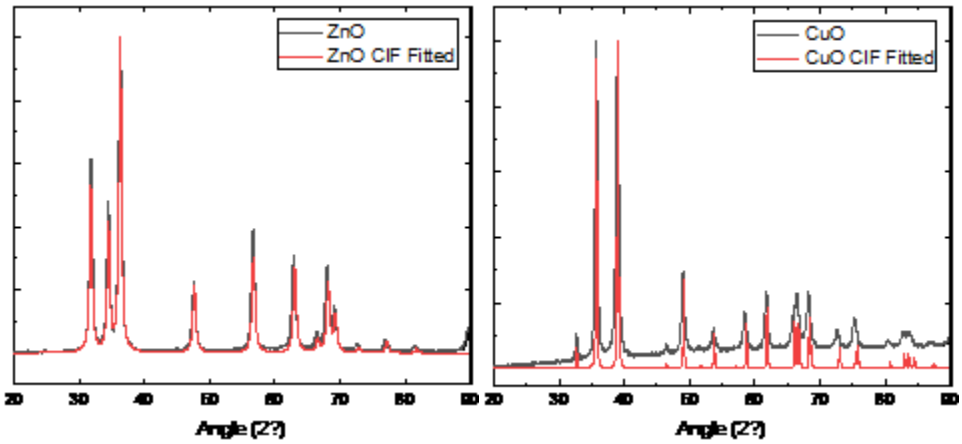


Figure 2. X-ray Diffraction (XRD) Plot for ZnO (left) and CuO (right). Red lines (ZnO CIF fitted and CuO CIF Fitted) include standard library peaks for ZnO and CuO, respectively. Black lines (ZnO and CuO) were obtained from our MONPs.

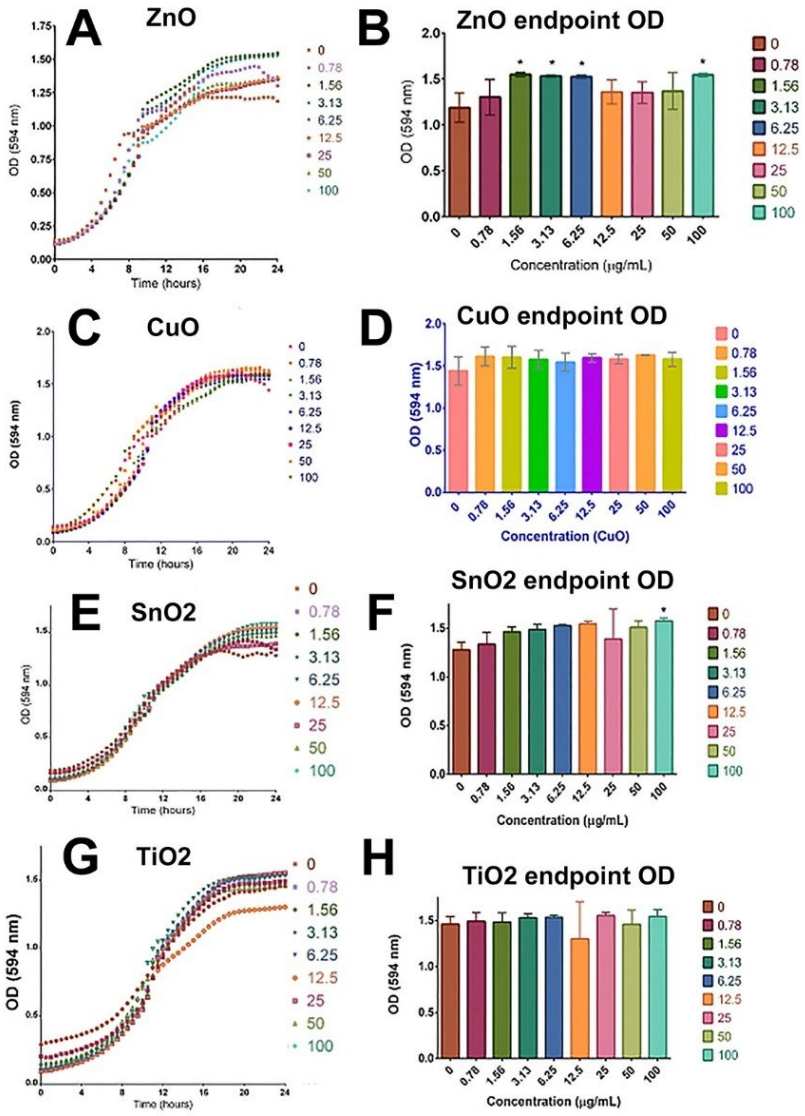


Figure 3. Cell Viability Measurement After 24 h of Treatment. ZnO treatments (A,B). CuO treatments (C,D), SnO2 treatments (E,F), and TiO2 treatments (G,H). Asterisks were used to identify values significantly different. This experiment was repeated many times but one representative is shown. One asterisk (*) indicates $p < 0.05$.

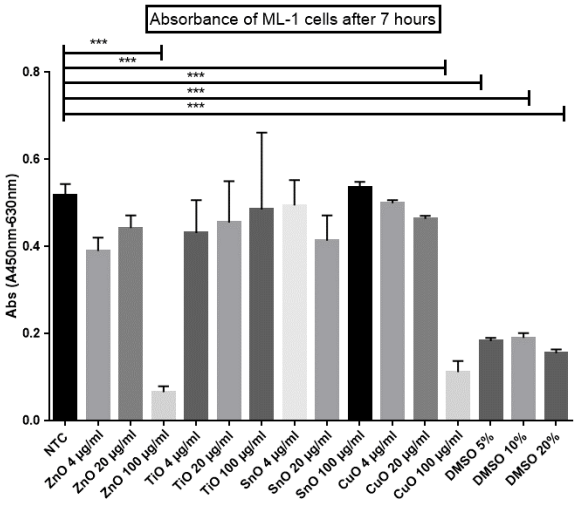


Figure 4. Effects of ZnO, CuO, TiO2, and SnO2 on ML-1 Cell Viability. DMSO serves as a positive control. Statistically significant results are indicated based on p-values: *** $p < 0.001$.

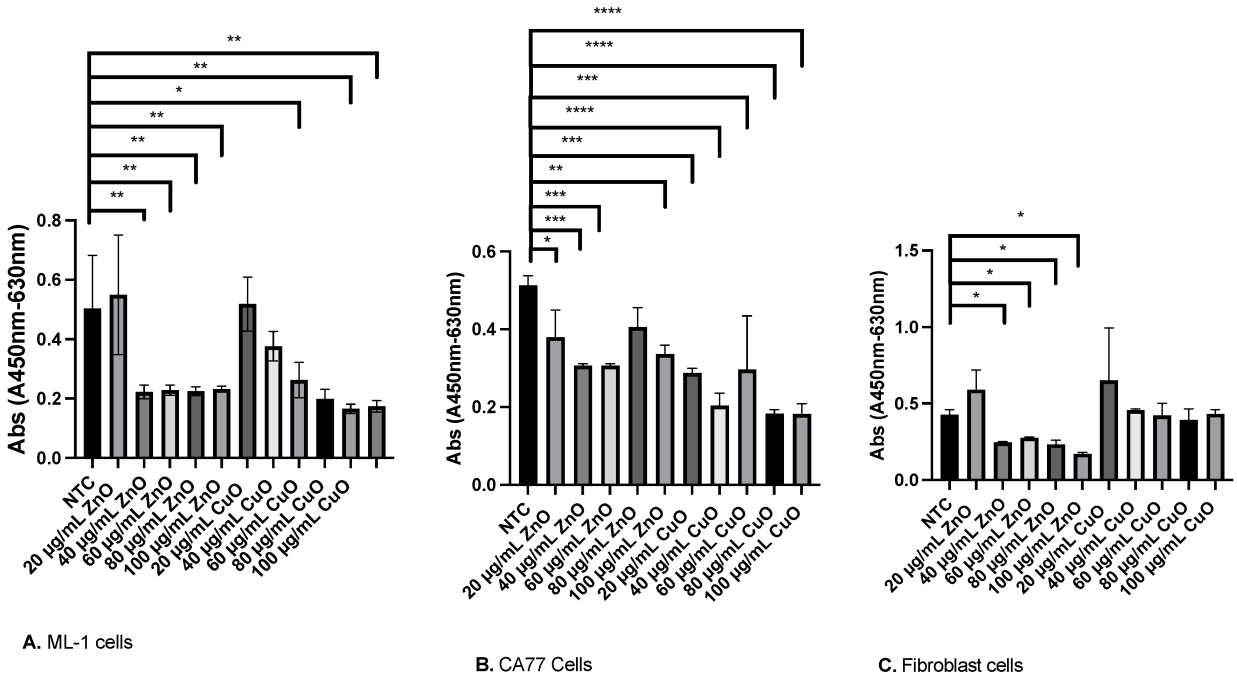


Figure 5. Minimal Inhibitory Concentration (MIC) for ZnO and CuO. (A) ML-1 cells exhibited decreased viability. (B) CA77 cell viability assay. (C) Viability of mouse fibroblast cells with various concentrations of ZnO and CuO. Statistically significant results are indicated based on p-values: * $p < 0.05$, ** $p < 0.01$, *** $p < 0.001$, and **** $p < 0.0001$.

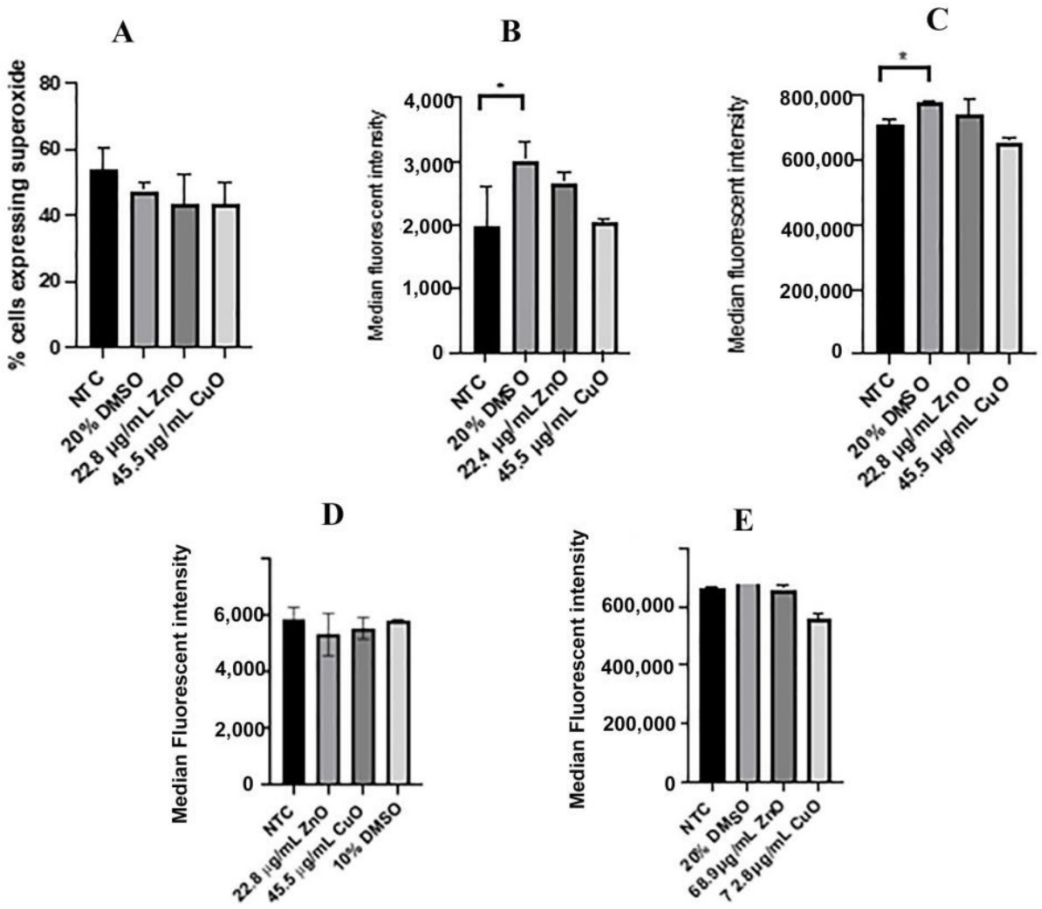


Figure 6. ML-1 and CA77 Cells Expressing Superoxide Production. (A) The percentage of ML-1 cells expressing superoxide after 24 h of treatment with 22.4 µg/mL ZnO or 45.5 µg/mL CuO. (B) Median superoxide production in ML-1 after 24 h. (C) Median superoxide production in ML-1 cells after 4 h. (D) Median superoxide production in n ML-1 cells after 30 min. (E) Median superoxide production in CA77 cells after 24 h. * indicates $p < 0.05$.

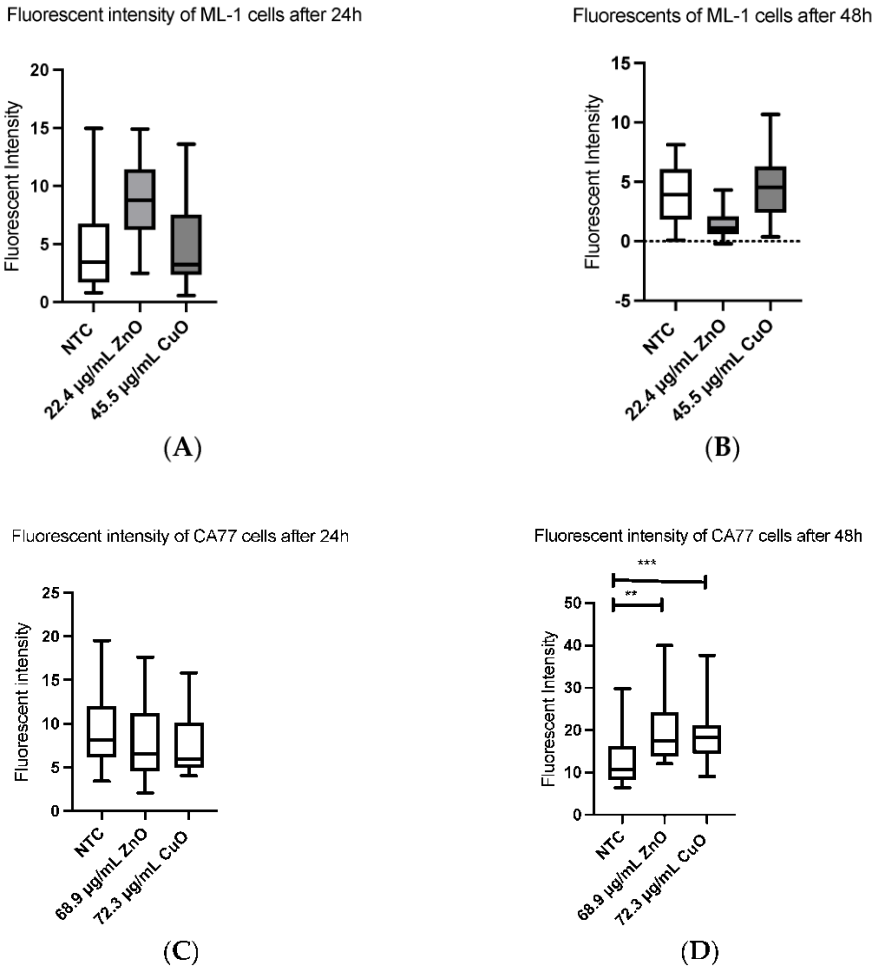


Figure 7. Levels of ROS Measured by CellROX Green Probe. (A) ML–1 cells with the indicated amount of MONPs after 24 h. (B) After 48 h of incubation with the same amounts as shown in (A). (C) After 24 h of incubation with ZnO and CuO treatment on CA77 cells. Then 48 h of treatment (D). Two asterisks (**) and three asterisks (***) indicate $p < 0.01$ and $p < 0.001$, respectively.

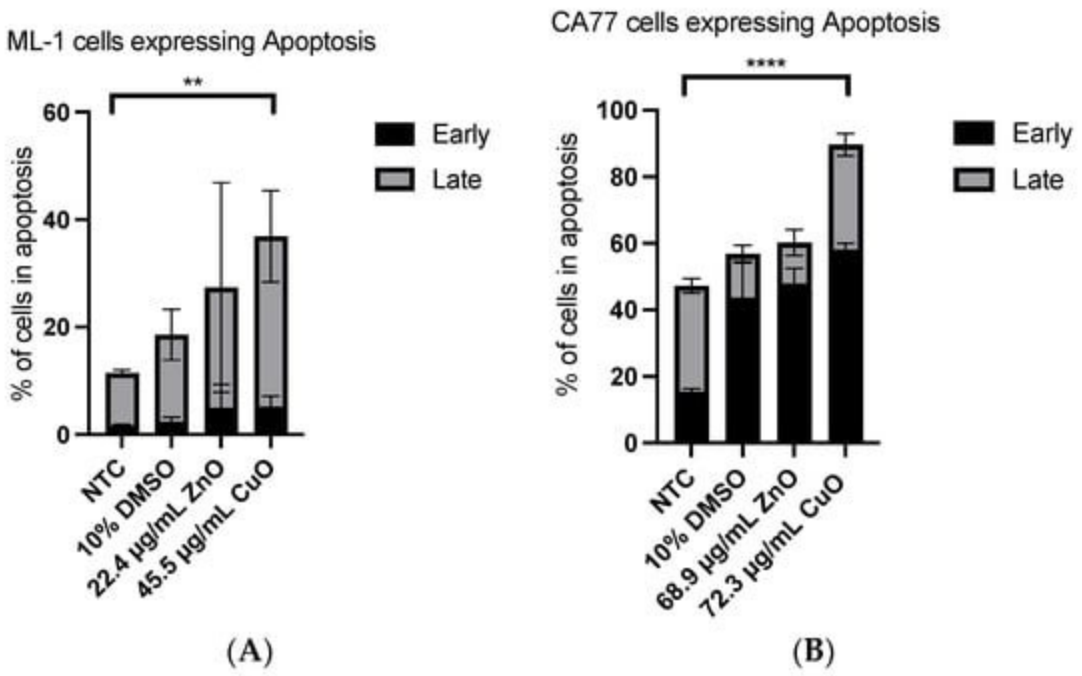


Figure 8. Quantitated Apoptosis with Two Different Cell Lines: ML-1 (A) and CA77 (B). Two asterisks (**) and four asterisks (****) indicate $p < 0.01$ and $p < 0.0001$, respectively

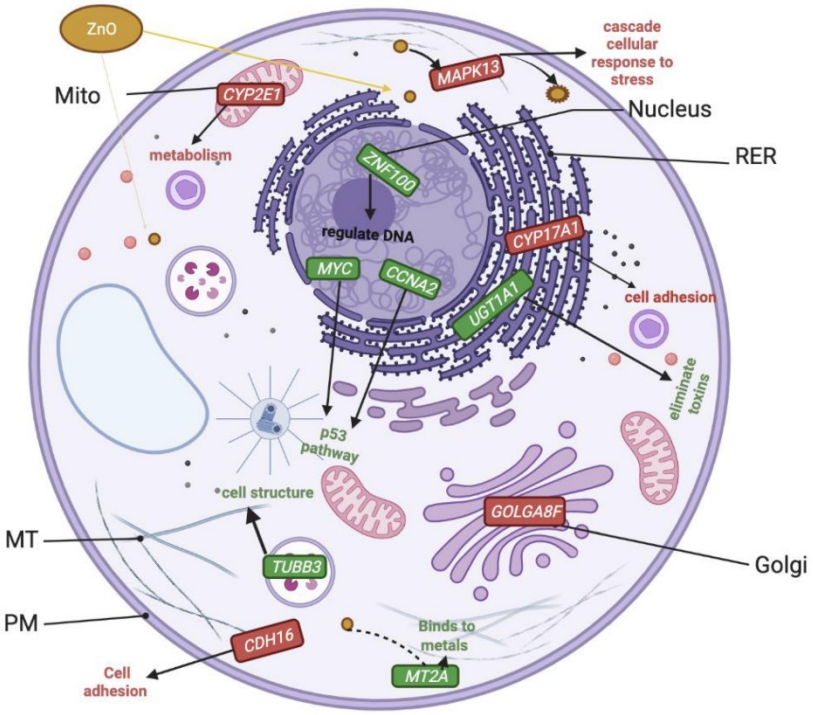


Figure 9. Cell Model Presents the Most Highly Upregulated (green) and Severely Downregulated Genes (red) in ML-1 Cells When Treated with ZnO. The most frequently up- or down-regulated biological pathways in response to ZnO in ML-1 cells are displayed in Table 1. ZnO-treated cells resulted in differentially expressed genes (DEGs) involved in p53 (MYC and CCNA2), heavy metal response (MT2A and ZNF100), cell stress (MAPK13 and UGT1A1), membrane trafficking (GOLGA8F and TUB3), metabolism (CYP2E1), and cell adhesion (CYP17A1 and CDH16).

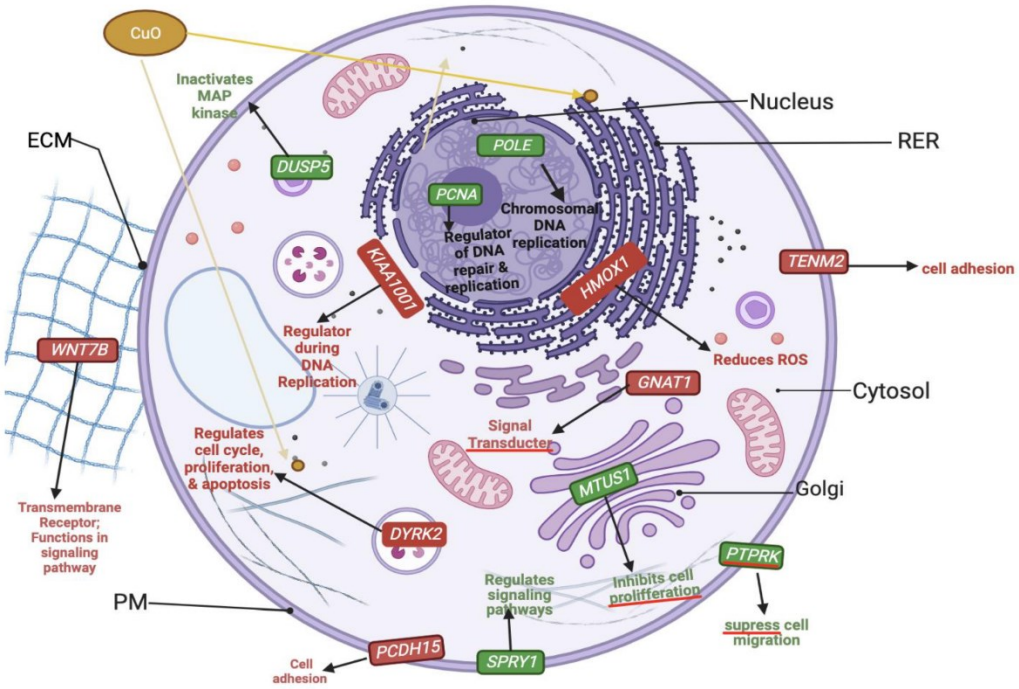


Figure 10. Cell Model Represents Significantly Upregulated Genes (green) and Severely Downregulated Genes (red) Expressed in ML-1 Cells When Treated with CuO. Please see Table 1 for the most frequently up- and down-regulated pathways. As shown here, genes implicated in DNA repair (POLE and PCNA) or proliferation inhibition (SPRY1, DUSP5, and MTUS1) are highly upregulated (more than >20-fold), while genes implicated in Wnt signaling (WNT7B) or cell adhesion (PCDH15 and TENM2) were significantly downregulated (>20-fold).

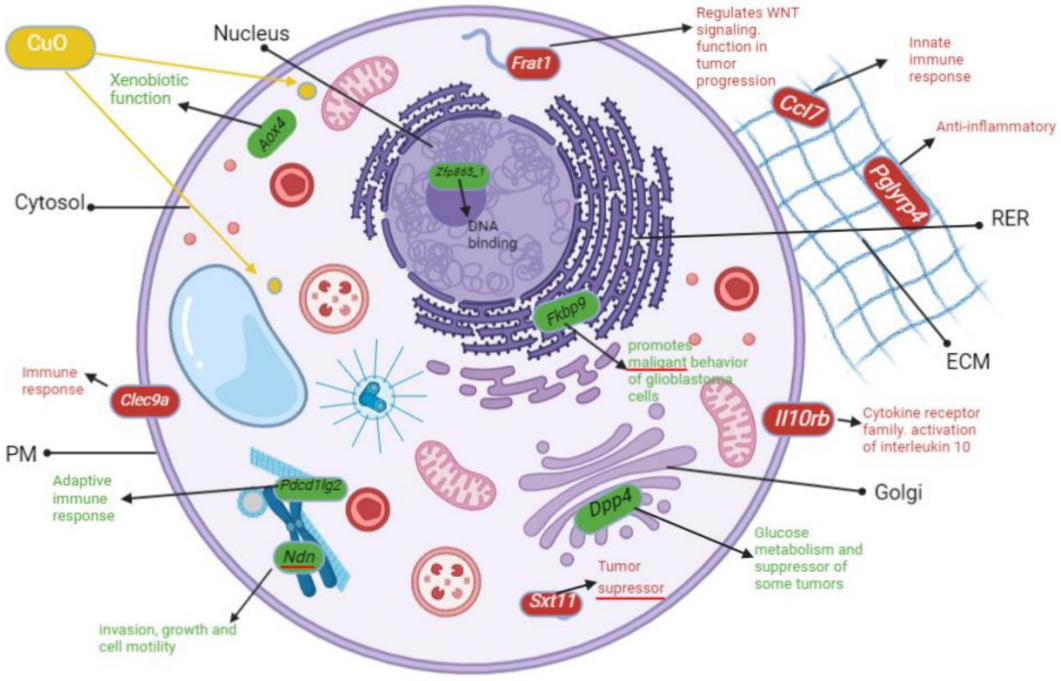


Figure 11. Cell Model Represents the Most Significantly Upregulated (green) and Severely Downregulated (red) Genes in CA77 Cells with CuO. The most frequently altered pathways can be found in Table 1. In particular, genes implicated in inflammation (Dpp4 and Pdcd1Ig2), xenobiotic function (Aox4), and transcription repressor (Zfp865_1) were upregulated more than 20-fold. In contrast, genes involved in Wnt signaling (Frat1), anti-inflammation (Pglyrp4), and cell growth (Il10rb) were severely downregulated.

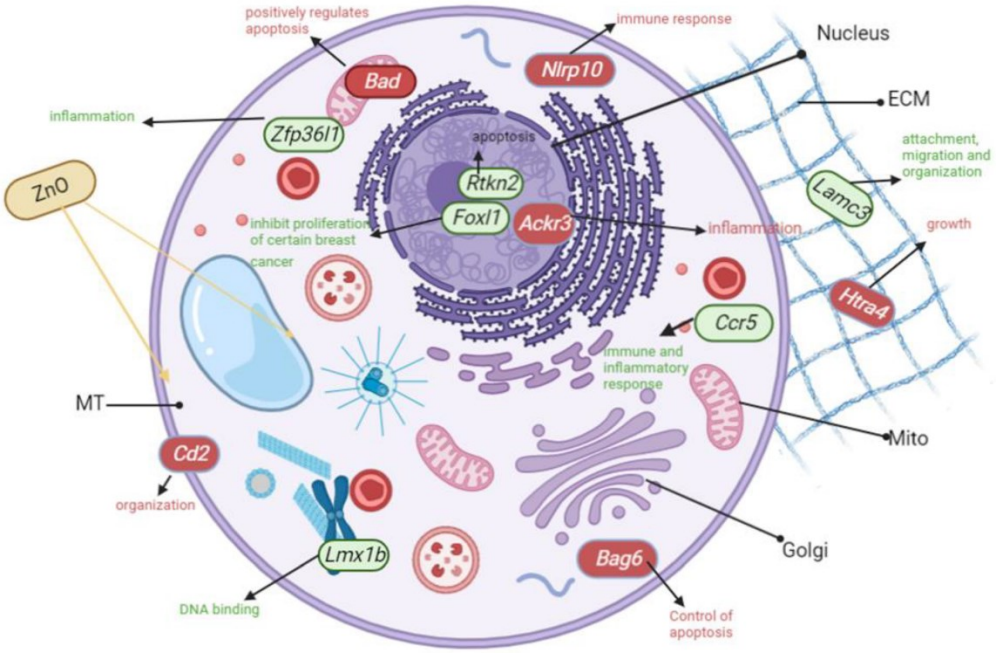


Figure 12. Cell Model Represents the Most Upregulated (green) and Severely Downregulated (red) Genes Expressed in CA77 Cells After ZnO Treatment. Table 1 contains biological pathways, most frequently up- or down-regulated.